Proceedings of the ASME 2013 Fluids Engineering Division Summer Meeting
FEDSM2013
July 07-11, 2013, Lake Tahoe, Nevada, USA

FEDSM2013-16503

PARTICLE TRANSPORT IN A TURBULENT SQUARE DUCT FLOW WITH AN IMPOSED MAGNETIC FIELD

Rui Liu
University of Illinois at Urbana-Champaign
Urbana, IL, USA, 61801

Surya P. Vanka
University of Illinois at Urbana-Champaign
Urbana, IL, USA, 61801

Brian G. Thomas
University of Illinois at Urbana-Champaign
Urbana, IL, USA, 61801

ABSTRACT

In this paper we study the particle transport and deposition in a turbulent square duct flow with an imposed magnetic field using Direct Numerical Simulations (DNS) of the continuous flow. A magnetic field induces a current and the interaction of this current with the magnetic field generates a Lorentz force which brakes the flow and modifies the flow structure. A second-order accurate finite volume method in time and space is used and implemented on a GPU. Particles are injected at the entrance to the duct continuously and their rates of deposition on the duct walls are computed for different magnetic field strengths. Because of the changes to the flow due to the magnetic field, the deposition rates are different on the top and bottom walls compared to the side walls. This is different than in a non-MHD square duct flow, where quadrant (and octant) symmetry is obtained.

INTRODUCTION

Particle transport in turbulent flows is important in various industrial applications, such as transport and entrapment of inclusion particles in continuous casting (CC) of steel. Quan, Vanka and Thomas [1, 2] conducted an LES simulation of the instantaneous liquid steel flow in a continuous caster mold region, in which inclusion particles were released from meniscus and upstream, and trajectories of particles were computed. A large number of studies on particle motion in wall-bounded turbulent flows and particle deposition onto solid walls were performed by previous researchers via numerical simulations. Among these, several studies of particle transport in turbulent flow in a square duct have been previously reported [e.g. 3-8].

Winkler, Rani and Vanka [3, 4] performed Large Eddy Simulations (LES) of particle transport in a square duct with varying particle Stokes numbers to investigate the preferential locations of the particles. They adopted one-way, two-way and four-way couplings between the fluid and the particle phase for different particle volume fractions. Their studies pointed out that the one-way coupling approach for particle simulation in a square duct flow is accurate for particle volume fractions less than 10^{-4}. They observed that the particle wall normal deposition velocity increases with particle Stokes number, and secondary mean flows cause a wavy pattern of particle deposition velocity across the duct width. Winkler, Rani and Vanka [3] also studied preferential particle concentrations for different particle Stokes numbers. Their results show that particles accumulate in regions with high compressional strain, and regions with low swirling strength. They demonstrated that vorticity is not always an accurate measure of preferential particle concentrations especially at the near wall region where swirl is dominated by shear.

Sharma and Phares [5, 6] subsequently performed a DNS of turbulent flows in a square duct with Lagrangian particle tracking to study the effects of particle inertia on the dispersion and deposition onto the duct side walls. They observed that higher-inertia particles tend to accumulate near the wall region and mix more efficiently along the longitudinal direction, while particles with lower inertia are more likely to be sent to the near wall region by the mean secondary flow and then drifted back to the main stream, which is called particle resuspension. Yao et.al. [7] also investigated particle resuspension in turbulent square duct flow with a relatively high bulk Reynolds number of 250,000 using LES and a dynamic SGS model [9]. They found that for small particles, particle resuspension is dominated by drag force, and the secondary flow; while for large particles, lift force cannot be neglected. They also evaluated the effect of gravity on particle resuspension, and concluded that gravity acts against particle resuspension.

Electromagnetic devices are sometimes utilized to control the flow behavior of magnetic conducting fluids in industrial applications, such as MHD pump and Electro-Magnetic Brake (EMBr) in continuous casting of liquid steel. It is found that when the flow is turbulent, the fluctuations are selectively damped by the magnetic field to the extent the turbulence becomes two-dimensional. Chaudhary et.al. [10] performed LES simulations of liquid metal flow in a scaled model of continuous casting mold region, where they studied EMBr effects on the flow patterns in the mold region. Chaudhary, Vanka and Thomas [11] performed DNS simulations of the turbulent flow of a magnetically-conducting fluid in a square duct with an imposed magnetic field. The modified turbulence field influences the mixing, particle transport and heat transfer to the walls. The modification of the (secondary) mean flow field as well as near-wall turbulence by the imposed magnetic field is presented in this detailed study. As observed by many researchers [3-8] since the secondary flow significantly affects the pattern of particle deposition on square duct walls, and the applied magnetic field has a significant influence on the flow field, the particle dispersion and deposition in turn are also affected. Thus, study of particle behavior in turbulent flows with the effect of imposed magnetic field is of importance both fundamentally and practically.

In this work, particle dispersion and deposition in the turbulent square duct flow at Re_τ=360 with and without magnetic field effects are investigated via DNS. A pressure-based finite volume approach and a Lagrangian particle tracking scheme are implemented on a Graphic Processing Unit (GPU). An in-house GPU-based code CU-FLOW was first used in the simulations to calculate square duct turbulent flows with and without MHD effects. Subsequently these flows were used to compute particle transport for two different particle response times. The preferential particle deposition locations, particle deposition velocities, and particle dispersion are analyzed and presented.

NUMERICAL FORMULATION

Governing equations

Three sets of coupled equations are solved which describe the three different aspects of physics in this problem: the continuity and Navier-Stokes equations for the turbulent fluid flow, equation for the electric potential, and equation for particle motion.

Equation for Fluid Flow

Isothermal incompressible flows are governed by the continuity equation and Navier-Stokes equations given by equation (1) and (2) below:

$$\nabla \cdot \mathbf{u} = 0 \tag{1}$$

$$\rho\left(\frac{\partial \mathbf{u}}{\partial t} + \nabla \cdot (\mathbf{uu})\right) = -\nabla p + \mu \nabla^2 \mathbf{u} + \mathbf{f} \tag{2}$$

MHD Equations

For flows with MHD effects, an additional term with the Lorentz force is added to the Navier-Stokes equations. The Lorentz force is calculated in equation (3) with local current, J, and imposed magnetic field, $\mathbf{B}_0$. The current in equation (4) is obtained from electric potential and instantaneous velocity field, where the electric potential field is solved from a Poisson equation as shown in (5).

$$\mathbf{f} = \mathbf{J} \times \mathbf{B}_0 \tag{3}$$

$$\mathbf{J} = \sigma\left(-\nabla \phi + \mathbf{u} \times \mathbf{B}_0\right) \tag{4}$$

$$\nabla^2 \phi = \nabla \cdot \left(\mathbf{u} \times \mathbf{B}_0\right) \tag{5}$$

3. Equation for Particle Motion

Calculations of particle motion are usually based on the formulation by Maxey and Riley [12] for the forces acting on a rigid sphere in a nonuniform flow. These include the drag force, lift force, gravitational force, pressure and stress gradient force, Basset history force, and added mass force. Elghobashi and Truesdell [13] showed that for heavy particles (particles with high particle to fluid density ratio), only the drag force, buoyancy force and Basset history force are important for particle transport. However, they also pointed out that the Basset history force due to fluid acceleration is usually an order of magnitude smaller than the drag force. Thus in current study, only the drag force and the lift force are taken into consideration, while other forces are neglected.

Particle trajectories can be integrated from instantaneous particle velocities in the flow field via equation (6), and particle velocities are computed by solving the force balance equation as shown in equation (7) below:

$$\mathbf{v}_p = \frac{d\mathbf{x}_p}{dt} \tag{6}$$

$$m_p \frac{d\mathbf{v}_p}{dt} = \mathbf{F}_D + \mathbf{F}_L \tag{7}$$

The two terms on the right hand side (RHS) of equation (7) are the drag force and lift force. The drag force is calculated by equation (8), where the drag coefficient from Schiller and Naumann [14] is calculated via a correlation with particle Reynolds number as shown in (9).

$$\mathbf{F}_D = \frac{\pi}{8} d_p^2 \rho C_D \left|\mathbf{u} - \mathbf{v}_p\right| \left(\mathbf{u} - \mathbf{v}_p\right) \tag{8}$$

$$C_D = \frac{24}{Re_p}\left(1 + 0.15 Re_p^{0.687}\right), \qquad Re_p = \frac{\rho\left|\mathbf{u} - \mathbf{v}_p\right| d_p}{\mu} \tag{9}$$

The lift force is calculated by the relation proposed by Saffman [15] given by equation (10):

$$\mathbf{F}_L = 1.61 d_p^2 \left(\rho\mu\right)^{0.5} \left|\nabla \times \mathbf{u}\right|^{-0.5} \left[\left(\mathbf{u} - \mathbf{v}_p\right) \times \left(\nabla \times \mathbf{u}\right)\right] \tag{10}$$

The particle response time is defined in equation (11), which reflects the time needed for a particle to accelerate from stationary state to about 0.632 of surrounding fluid velocity.

$$\tau_p = \frac{\rho_p d_p^2}{18\mu} \tag{11}$$

The particle Stokes number is defined as the dimensionless particle response time in wall units, as shown in equation (12) below:

$$\tau_p^+ = \frac{\tau_p u_\tau^2}{\nu} \tag{12}$$

Physical Domain and Boundary Conditions

The solution domain considered here for fluid flow and particle transport has dimensions of $L_x \times L_y \times L_z = 8\times1\times1$, for the streamwise ($x$-axis), spanwise ($y$-axis) and transverse ($z$-axis) directions respectively. The imposed magnetic field is along the positive z-axis direction, pointing from the bottom wall to the top wall of the square duct.

Fluid-phase Boundary Conditions

Periodic boundary conditions in the streamwise direction and no-slip wall boundaries at all four side walls are therefore prescribed. For the electric potential, since no current penetrates the duct walls, a Neumann boundary condition is prescribed.

At wall y=0 and y=1, $u_y = 0$, $\dfrac{\partial\phi}{\partial y} = 0$;

At wall z=0 and z=1, $u_z = 0$, $\dfrac{\partial\phi}{\partial z} = 0$.

Particle Boundary Conditions

In previous studies [3-7], periodic boundary conditions were adopted for particle transport in a square duct. However, this treatment of particle boundary conditions has two issues: first, particles initially put in the domain will continuously deposit to the side walls. Eventually all particles will be deposited onto the side walls, which suggests that the particle volume fraction in the domain keeps decreasing with time, while for parametric studies, it is desirable to keep particle volume fraction constant in each individual case; second, it creates certain difficulty in studying particle dispersion along the longitudinal direction of the square duct, since particles distributed at different locations initially in the domain will travel at different streamwise velocities, and particles close to the wall region will have much lower streamwise velocities compared with particles at the core region. Then the number of "duct length" has to be counted for each particle in order to study particle dispersion and deposition along the longitudinal direction.

Thus, in this work, boundary condition for the particle phase in streamwise direction is defined such that particles enter the computational domain at a constant rate, which leads to a specific particle volume fraction in the domain. The initial locations of particles at domain inlet with x=0 are randomly distributed, and the initial particle velocities are set to be equal to the local fluid instantaneous velocity. When a particle travels out of the computational domain, it never comes back to the domain as in the periodic boundary condition case. New particles are released from a random location at the cross section of x=0.

Particle boundary conditions at side walls are set to be completely absorbing: once the distance between the center of particle and the wall is less than the particle radius, the particle is considered to be deposited on the duct wall.

Numerical Schemes

The coupled equations between fluid flow and MHD are discretized with 512×80×80 cells in a Cartesian coordinate system, and the solution fields are obtained using a pressure-based finite-volume approach. The convection-diffusion terms in the momentum equations are discretized using a second-order Adams-Bashforth scheme. A fractional step method is used to project the pressure field to a divergence-free space, and resultant pressure Poisson equation is solved using a geometric multi-grid technique, with red-black Gauss-Seidel relaxation. Electric potential is solved in a similar manner, as described by Chaudhary [10, 11].

The equation for particle motion is discretized and solved in a Lagrangian particle-tracking approach. Particle position is obtained using a 1st order Euler scheme, and the particle velocity is integrated using a 4th order Runge-Kutte scheme. Interpolation of grid velocities onto particle locations is achieved using the 3-D Lagrange cubic interpolation function from a 3×3×3 cell block surrounding the particle, as shown in equation (13), and the Lagrange multipliers are defined in equation (14).

$$\varphi_p = \sum_{n=1}^{27} L_x^{ni} L_y^{nj} L_z^{nk} \varphi_n \tag{13}$$

$$L_x^{ni} = \prod_{i=1, ni\neq i}^{3} \frac{\left(x_p - x_i\right)}{\left(x_{ni} - x_i\right)},$$

$$L_y^{nj} = \prod_{j=1, nj \neq j}^{3} \frac{(y_p - y_j)}{(y_{nj} - y_j)},$$
$$L_z^{nk} = \prod_{k=1, nk \neq k}^{3} \frac{(z_p - z_k)}{(z_{nk} - z_k)}. \quad (14)$$

RESULTS AND DISCUSSIONS

The discretized set of Navier-Stokes equations, MHD equations and particle transport equations are solved on a Tesla C2075 GPU. The fluid density is set to unity, and its dynamic viscosity is set to 0.00264. The Reynolds number based on wall friction velocity in current flow is 360, and the Hartman number in the MHD case is 21.2.

Two different particle response times were studied in current work both with and without magnetic fields, with the particle Stokes number being 5 and 15. The particle to fluid density ratio is kept 1000.0 constant, and the particle diameter varies between 0.000833 and 0.00144 to yield the different particle response times, 0.0146 and 0.0439 (corresponding to particle Stokes number of 5 and 15 respectively). The particle volume fractions for the two different particle Stokes numbers of 5 and 15 are 1.89×10^{-5} and 9.84×10^{-5} respectively, both kept below 10^{-4}, in order to hold the one-way coupling assumption.

Comparison of Flow Fields with and without MHD effects

Both instantaneous and mean velocity fields are plotted in Figures 2 and 3, for cases with and without imposed magnetic field. Figure 2(a) and (b) compare the secondary instantaneous flows at a cross section of *x*=6 for cases with/without magnetic effects, where in the case with magnetic field, the turbulent eddies close to the top and bottom duct walls are suppressed compared with the non-MHD case, as already reported by Chaudhary et.al. [11].

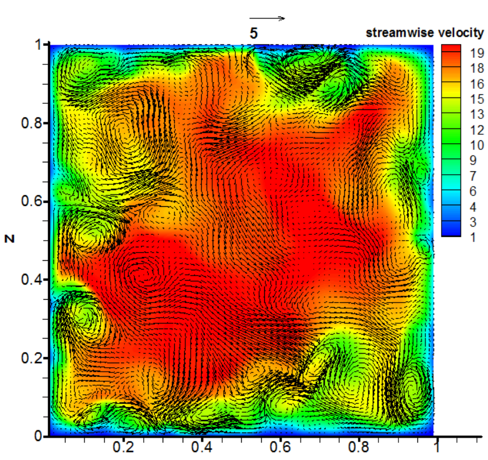

(a)

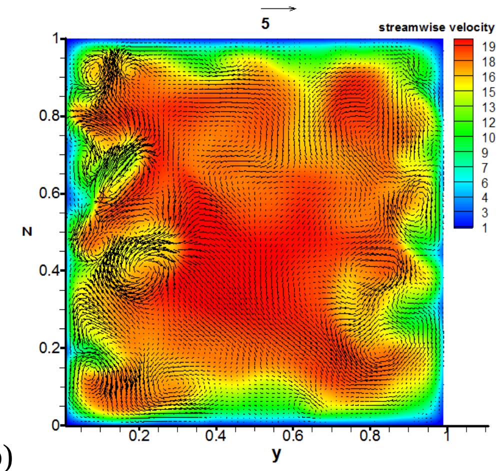

(b)

Figure 2. Instantaneous Velocity Field in Cross-Stream Direction: (a) without MHD; (b) with MHD

It is clearly shown from the mean velocity fields in Figure 3(a) and (b) that the mean secondary flows are greatly changed by addition of the magnetic field. The secondary mean flow eddies in the MHD case do not establish the symmetric feature about the corner bi-sector, instead, a stronger vortex near the top and bottom walls are generated and the eddies on the other side are weakened but get closer to the side walls. This change of secondary flow pattern will alter the pattern of particle deposition.

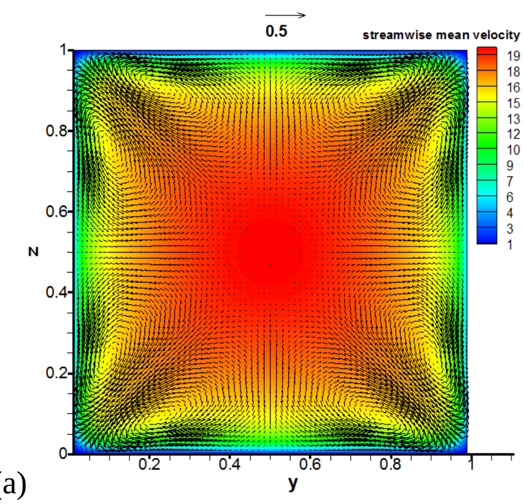

(a)

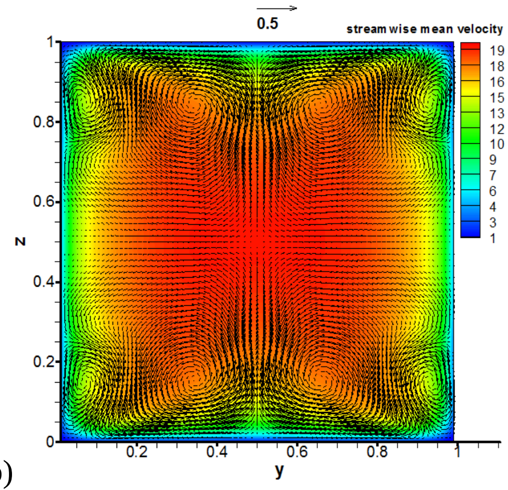

(b)

Figure 3. Mean Velocity Field in Cross-Streamwise Direction: (a) without MHD; (b) with MHD

Particle Deposition

In this section, we present the particle deposition probability density and locations of preferential deposition. In order to quantify the particle deposition, the particle deposition probability density function is defined by the following equation (15).

$$pdf = \frac{N_d A}{\dot{N}_{in} \Delta t V} \tag{15}$$

In order to numerically obtain a distribution of particle deposition over the wall locations, each duct wall is divided into 200 bins along the streamwise direction, and the number of particles in each of the bins is counted. The particle number is then divided by the time needed for the deposition to occur, and corresponding length scale of the bin to calculate the local pdf of the deposition .

The probability density function of particle deposition along the streamwise direction is shown in Figure 4, for the two particle Stokes numbers with and without MHD effects. The deposition rate of particles is decreased by more than 50% by the imposed magnetic field, for both Stokes numbers of 5 and 15. The deposition rate also decreases with the streamwise location along the square duct in all four cases. This is due to the decrease in the number of the travelling particles. Increase of the slope close to the domain inlet is also observed. This might be caused by the random introduction of particle locations at domain entrance. This initial condition effect vanishes after x=0.5 along the streamwise direction.

Particle deposition rate increases significantly with the particle response time, or the particle Stokes number, by approximately one order of magnitude in both cases with and without MHD effects. As noticed by Brooke et.al. [16], two different mechanisms are responsible for the particle deposition in wall bounded turbulent flows. For particles with higher inertia, they have the energy to penetrate the boundary layer, and get deposited quickly, as described by the “free-flight” model [16]. For low inertial particles, the dominant way of deposition is through the turbulence diffusion. As the particle Stokes number increases from 5 to 15, inertial effect becomes more important in determining the deposition of particles.

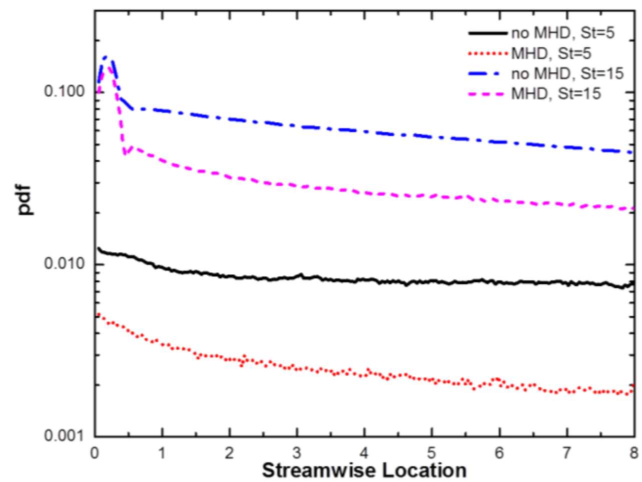

Figure 4. *PDF*s of Particle Deposition Location along Streamwise Direction

The distributions of particle deposition *pdf* along the y- and z-axis direction at four side walls are plotted in Figure 5 (a) and (b). Note that *pdf* distribution of particles deposited on opposite walls are supposed to be statistically identical. Thus the particle deposition *pdf* presented in Figure 5 is averaged over opposite walls.

Figure 5(a) shows the particle deposition *pdf* on the left-right side walls (with y=0 and y=1). It is observed that for all four cases, the deposited particles preferentially concentrate in regions close to the corner and in the middle part of the wall. A wavy pattern for the preferential depositing locations is observed. For cases without MHD effects, particle deposition *pdf* patterns on left-right and bottom-top side walls reflect each other, as could be expected. Higher particle response time, or Stokes number, tends to make the deposition patterns less preferential, but more uniform (black solid line and blue dashed line).

The most biased deposition between the left-right and bottom-top side walls occurs in the MHD case with particles of smaller Stokes number (St=5). In this case, particles deposited on the side walls exhibit a similar but more wavy distribution with the non-MHD flow cases, while the top and bottom wall particle depositions show peaks near the two corners, with low particle deposition rate in the middle region (between 0.2 and 0.8) on the wall. The particle number density in this region is just 5% of that in the non-MHD flow case.

For the MHD case with higher particle response time (St=15), the *pdf* distribution between left-right and bottom-top walls is less biased compared to the case with smaller particle response time. Particle distribution near corner regions is similar for left-right and bottom-top walls. However, the shape of particle depositing *pdf* curve flipped in the center region of the wall, with higher depositing ratio on left-right side walls than bottom-top walls.

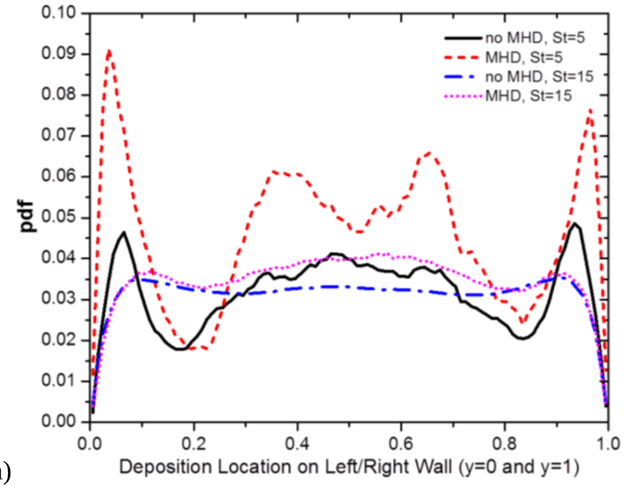

(a)

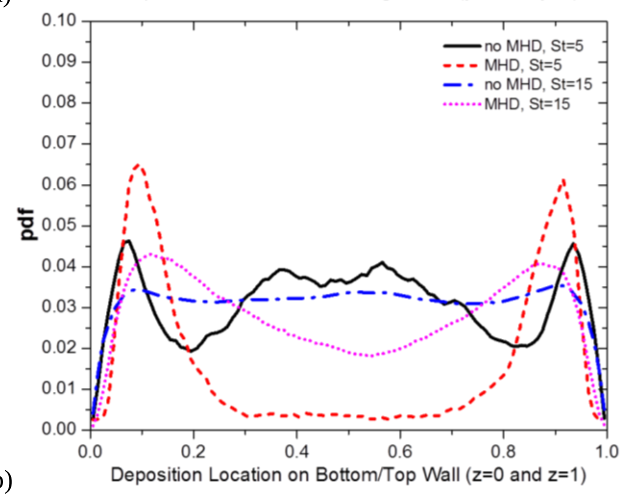

(b)

Figure 5. *PDF*s of Particle Deposition Location along Spanwise and Transverse Directions

Figure 6 (a-b) and Figure 7 (a-b) show the distributions of deposited particles on the square duct side walls in cases with and without MHD effects for the lower particle response time (S_t=5). It shows clearly again that the wall-deposited particle distributions on left/right walls (y=0 and y=1) and bottom/top walls (z=0 or z=1) for non-MHD square duct flows are similar to each other, while for MHD flows the particle deposition on wall z=1 (or z=0) are significantly altered from the non-MHD flow case. Very few particles deposit in the middle region of the wall in the MHD case. Deposited particles at bottom/top walls tend to accumulate to regions close to the duct corners. Particle deposition at left/right walls is exhibiting a streaky pattern in both cases with/without MHD effects.

Particle deposition velocity is another important factor to study. Figure 8 and Figure 9 side-by-side show the wall-normal and streamwise velocity distributions of depositing particles. In all cases, the streamwise velocities of depositing particles are more than one order of magnitude larger than the wall-normal velocities. The averaged wall-normal and streamwise velocities of the local fluid are also shown as a reference.

For the non-MHD flow case, the wall-normal particle deposition velocity has a higher value near the corners and around the middle regions of the walls, while the streamwise deposition velocity attains its maximum only at the middle region of the duct wall. In the MHD flow, both wall-normal and streamwise velocity distributions at bottom-top walls (z=0 and z=1) have peaks near the two duct corners, but very low deposition velocities in the middle part of the wall (between 0.3 and 0.8 along spanwise direction). Both wall-normal and streamwise velocities in MHD flows are much smaller compared with those from non-MHD flow case, especially in the middle part of the duct walls.

The near-wall averaged fluid velocities are taken from a distance of 3.67 wall units away from the wall. The wall-normal fluid velocities are much smaller than the wall-normal velocities of depositing particles. In all cases, particle depositing velocities increase with particle Stokes number in the same manner, as a result of the increased inertial effects of particles.

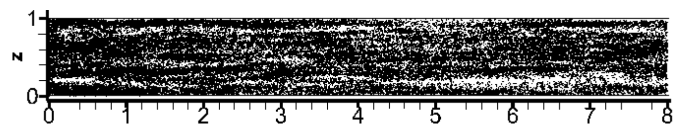

(a) Particle Deposition at wall y=0, no MHD

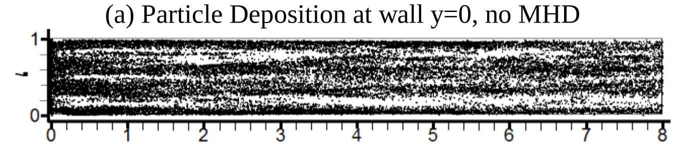

(b) Particle Deposition at wall y=0, with MHD

Figure 6. Particle Deposition Locations at Wall y=0 (S_t=5)

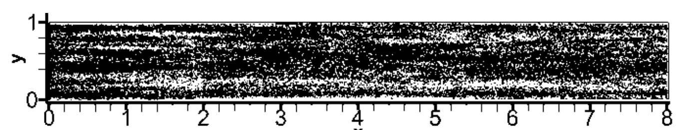

(a) Particle Deposition at wall z=1, no MHD

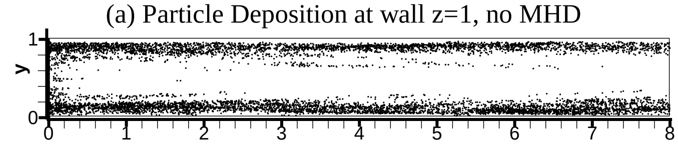

(b) Particle Deposition at wall z=1, with MHD

Figure 7. Particle Deposition Locations at Wall z=1 (S_t=5)

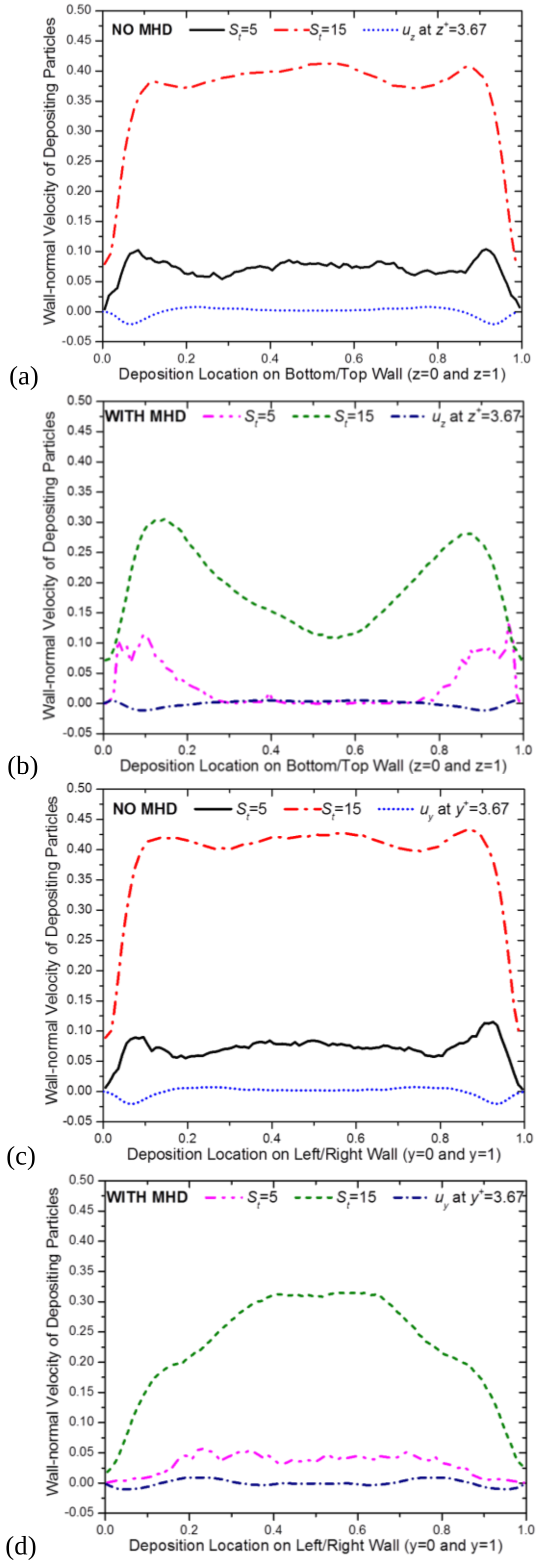

Figure 8. Wall-normal Velocity Distribution of Depositing Particle

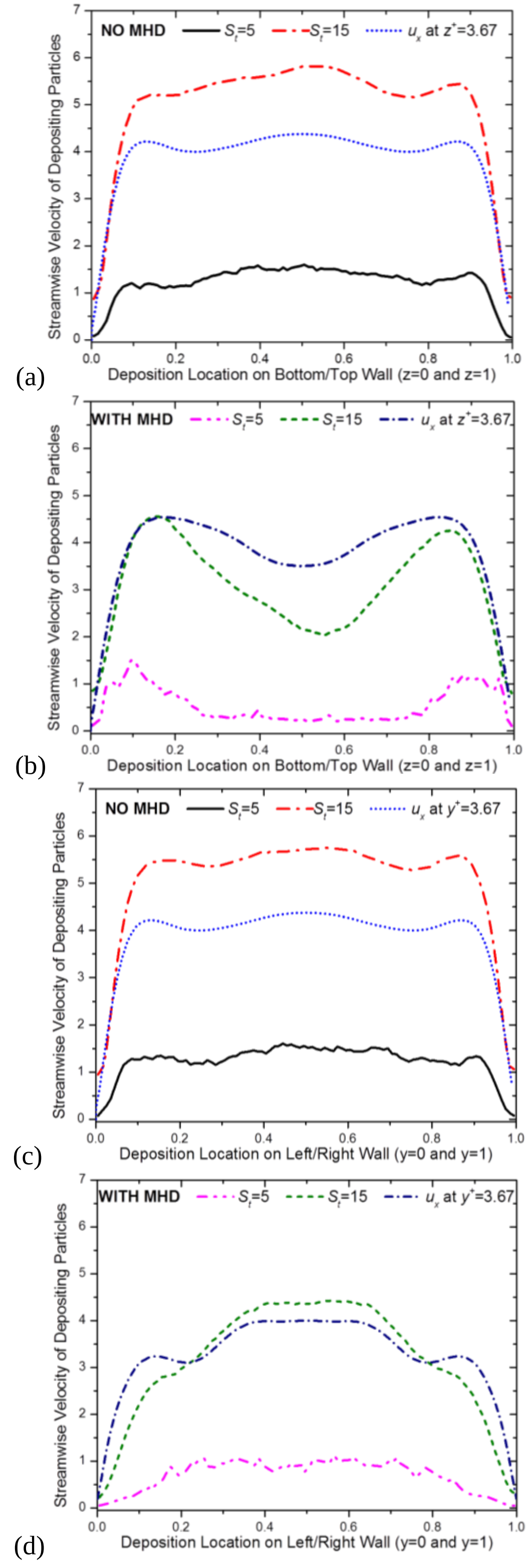

Figure 9. Streamwise Velocity Distribution of Depositing Particles

Particle Dispersion

The particle distributions at different cross-stream (x=6.0) slices of the square duct are plotted in Figure 10, together with fluid velocity vectors. Points in the plots represent particles dispersed within a Δx^+=7.5 fluid layer. Figure 10 (a-d) show that particles accumulate preferentially in the saddle regions of the flow in between the secondary turbulent eddies, and very few particles penetrate into the vortex centers of the secondary flow. Clustering of particles seems to be more obvious for larger Stokes number.

Streamwise velocity contours located at z^+=5 and y^+=5 slices are shown in Figure 11 and 12, together with the particle distribution within a thin layer of Δz^+=5 and Δy^+=5. It seems that particles accumulate preferentially in the transition regions between higher and lower velocity streaks. Comparison of particle distribution in the non-MHD flow (Figure 11(a)) and that in the MHD flow (Figure 11(b), (c)) with a particle Stokes number of 5 indicates that the streaky structures in MHD flows are thinner and more elongated than those in the non-MHD square duct flows, as reported by Chaudhary et.al. [11], resulting in a region with more concentrated particle dispersion, shown in Figure 12(b) and (c). Comparing the particle dispersion in Figure 11 (a-d, St=5) with Figure 12 (a-d, St=15), it is observed that for a larger particle response time, the number of particles dispersed within the same fluid layer decreases, due to the increase of particle deposition rate at higher Stokes number. The distribution of particles with St of 15 shown in Figure 12 (a-c) is more random than that in the St=5 case, suggesting the inertial effects on the preferential particle dispersion locations. The difference in the particle deposition mechanisms can also be inferred from the particle dispersions very close to the wall as shown in these two figures. Particles with smaller response times are drifted to the region very close to the duct walls, and then deposit from turbulence diffusion. Particles with higher inertia, on the other hand, obtain enough energy from the core region, and then penetrate the turbulent boundary layer and get deposited.

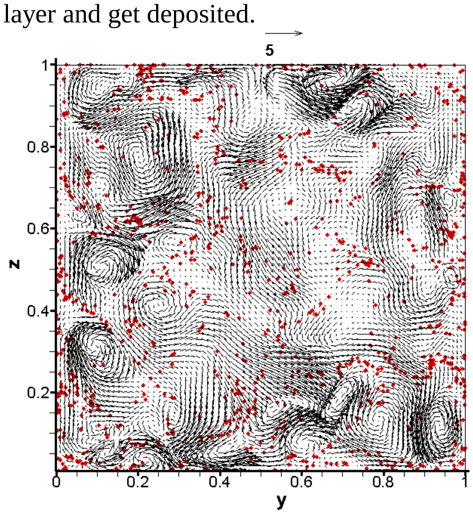

(a) without MHD, **(S_t=5)**

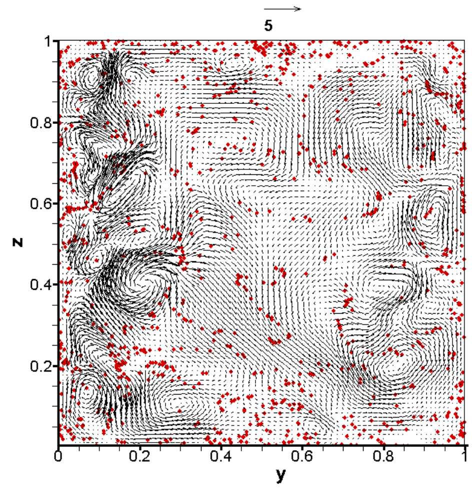

(b) with MHD, **(S_t=5)**

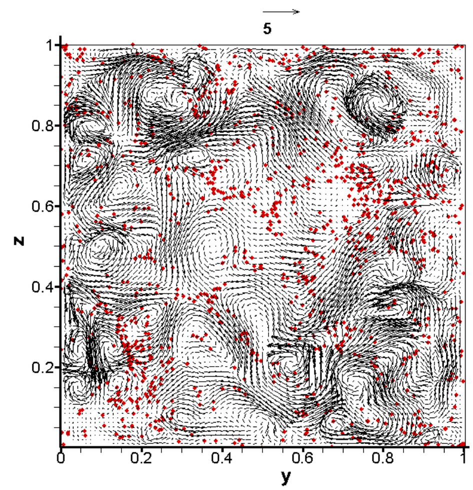

(c) without MHD, **(S_t=15)**

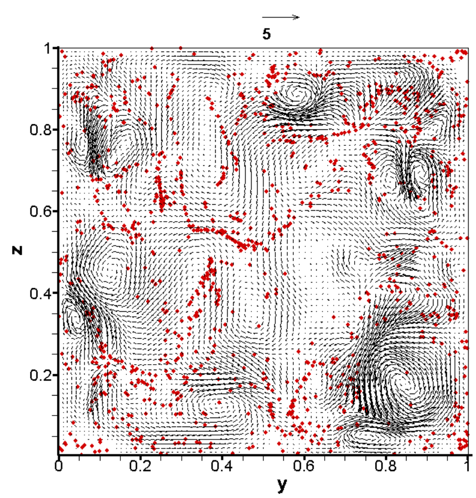

(d) with MHD, **(S_t=15)**

Figure 10. Particle Dispersion in Cross-Flow Plane

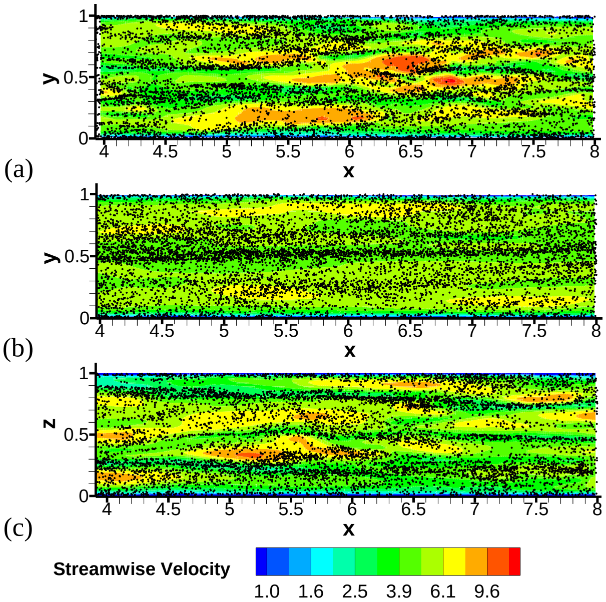

Figure 11. Instantaneous Streamwise Velocity Contours with Particle Distribution for S_t=5 (a) no MHD, (b) with MHD, at z^+=5, (c) with MHD, at y^+=5

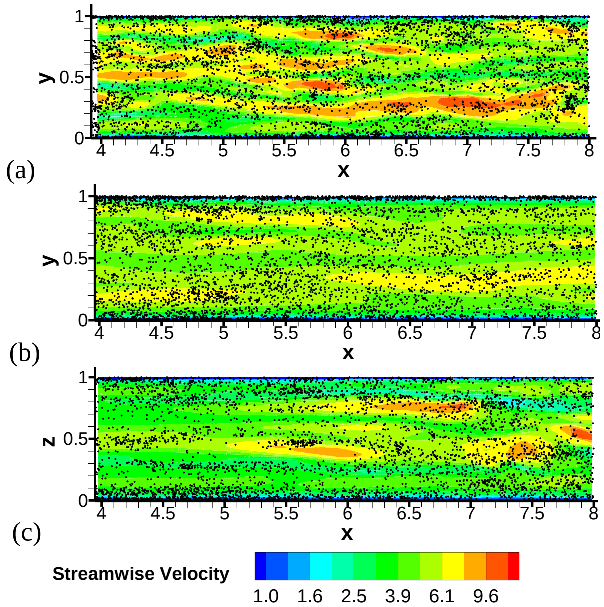

Figure 12. Instantaneous Streamwise Velocity Contours with Particle Distribution S_t=15 (a) no MHD, (b) with MHD, at z^+=5, (c) with MHD, at y^+=5

CONCLUSIONS

In this work, a DNS study on turbulent flow in a square duct with the effects of imposed magnetic field was first performed, and then Lagrangian particle tracking was utilized to investigate particle deposition and dispersion in the square duct.

Inclusion of magnetic field modifies the mean flow in the streamwise direction as well as secondary mean flows. Turbulence is suppressed with the effect of imposed magnetic field. Resultant secondary mean flow does not exhibit any more a symmetric pattern along the corner bi-sector.

Particle tracking results suggest that the pattern of particle deposition on the duct walls changes significantly with imposed magnetic field, with the particle deposition rate decreased from ~7% to ~2% (St=5). Preferential particle deposition location for no MHD case is observed to have a wavy shape along the spanwise direction, with more particles deposited near the corner region, and in the middle part of the wall. Similar deposition pattern is found at walls parallel to the direction of imposed magnetic field for the MHD case. However, at walls perpendicular to the magnetic field direction, the number of deposited particles decreases substantially at the middle region, while more particle can be found near the corner of the duct. Increasing particle Stokes number increases particle deposition rate and particle deposition velocities in both MHD and non-MHD cases. The average streamwise velocities of depositing particles are smaller than the local averaged fluid velocities at 3.67 wall units for the St=5 particles, but larger for the St=15 particles. In both MHD and non-MHD square duct flows, particles tend to accumulate in the saddle regions between turbulent eddies, but away from the centers of the secondary vortices of the cross-flow direction. Along the streamwise direction close to the wall, particles tend to gather in the transition regions between the high and low velocity streaks.

ACKNOWLEDGMENTS

The authors would like to thank the Continuous Casting Consortium, Department of Mechanical Science and Engineering, University of Illinois at Urbana-Champaign, IL, USA, and the National Science Foundation (Grant CMI 11-30882) for the support of current research. The assistance of Ramnik Singh and Dr. Rajneesh Chaudhary in providing the MHD version of CU-FLOW is gratefully acknowledged.

NOMENCLATURE

x, *y*, *z*	coordinates of the Cartesian system
u	fluid velocity vector
v	particle velocity vector
t	time
p	pressure
f	the Lorentz force vector
J	current

$\mathbf{B_0}$	imposed magnetic field vector
$\mathbf{F}_D$	drag force
$\mathbf{F}_L$	lift force
m_p	mass of a particle
d_p	particle diameter
C_D	drag coefficient
u_τ	friction velocity
Re_p	particle Reynolds number
Re_τ	Reynolds number based on friction velocity
S_t	particle Stokes number
n	cell index (or cell number)
$L_{x,y,z}$	Lagrange interpolation factor
	probability density function
N_d	number of deposited particle
Δt	time span for particle deposition
A	characteristic area of particle deposition
V	characteristic volume of particle deposition
$\dot{N}_{in}$	particle in-coming rate at domain inlet

Greek Symbols

ρ	density (of fluid or particle)
μ	dynamic viscosity of fluid
ϕ	electric potential
σ	magnetic conductivity
ν	kinematic viscosity of fluid
τ_p	particle relaxation time
τ_p^+	dimensionless particle relaxation time, or S_t
φ	generic physical quantity

Subscripts

p	quantity related to particle
i, j, k	cell index

REFERENCES

[1] Yuan, Q., Thomas, B.G., and Vanka, S.P., 2004, "Study of Transient Flow and Particle Transport during Continuous Casting of Steel Slabs, Part 1. Fluid Flow", Metallurgical and Materials Transactions B, **35**(B):4, pp. 685-702.

[2] Yuan, Q., Thomas B.G., and Vanka S.P., 2004, "Study of Transient Flow and Particle Transport during Continuous Casting of Steel Slabs, Part 2. Particle Transport", Metallurgical and Materials Transactions B, 35(B):4, pp. 703-714.

[3] Winkler, C.M., Rani, S.L., and Vanka, S.P., 2004, "Preferential Concentration of Particles in a Fully Developed Turbulent Square Duct Flow", International Journal of Multiphase Flow, **30**(1), pp. 27-50.

[4] Winkler, C.M., Rani, S.L., and Vanka, S.P., 2006, "Numerical Study of Particle Wall-deposition in a Turbulent Square Duct Flow", Powder Technology, **170**(1), pp. 12-25.

[5] Phares, D.J. and Sharma, G., 2006, "A DNS Study of Aerosol Deposition in a Turbulent Square Duct Flow", Aerosol Science and Technology, **40**(11), pp. 1016-1024.

[6] Phares, D.J. and Sharma, G., 2006, "Turbulent Transport of Particles in a Straight Square Duct", International Journal of Multiphase Flow, **32**, pp. 823–837.

[7] Yao, J. and Fairweather, M., 2010, "Inertial Particle Resuspension in a Turbulent, Square Duct Flow", Physics of Fluids, **22**, 03303.

[8] Narayanan, C. and Lakehala, D., 2003, "Mechanisms of Particle Deposition in a Fully Developed Turbulent Open Channel Flow", Physics of Fluids, **15**(3), pp.763-775.

[9] Germano, M., Piomelli, U., Moin, P., and Cabot, W.H., 1991, "A Dynamic Subgrid-Scale Eddy Viscosity Model", Physics of Fluids, **3**, pp. 1760-1765.

[10] Chaudhary, R., Thomas, B.G., and Vanka, S.P., 2012, "Effect of Electromagnetic Ruler Braking (EMBr) on Transient Turbulent Flow in Continuous Slab Casting using Large Eddy Simulations," Metallurgical and Materials Transactions B, **43**B (3), pp. 532-553.

[11] Chaudhary, R., Vanka, S.P. and Thomas, B.G., 2010, "Direct Numerical Simulations of Magnetic Field Effects on Turbulent Flow in a Square Duct", Physics of Fluids, **22**:7, 075102,

[12] Maxey, M.R. and Riley, J.K., 1983, "Equation of Motion for a Small Rigid Sphere in a Nonuniform Flow," Physics of Fluids, **26**, pp. 883-889.

[13] Elghobashi, S. and Truesdell, G.C., 1992, "Direct Simulation of Particle Dispersion in a Decaying Isotropic Turbulence," Journal of Fluid Mechanics, **242**, pp. 655.

[14] Schiller, L., Naumann, Z., 1935, "A Drag Coefficient Correlation", Z. Ver. Deutsch. Ing., **77**, pp. 318.

[15] Saffman, P.G., 1965, "The Lift on a Small Sphere in a Slow Shear Flow," Journal of Fluid Mechanics, **22**, pp.385.

[16] Brooke, J.W., Hanratty, T.J., and McLaughlin, J.B., 1994, "Free-Flight Mixing and Deposition of Aerosols", Physics of Fluids, **8**(10), pp. 3404-3415.